journal

J. Am. Ceram. Soc., 97 [6] 1837–1840 (2014)
DOI: 10.1111/jace.12837

Photovoltaic Properties of Multiferroic $BiFeO_3/BiCrO_3$ Heterostructures

Joyprokash Chakrabartty,[‡,†] Riad Nechache,[‡,§] Shun Li,[‡] Mischa Nicklaus,[‡] Andreaus Ruediger,[‡] and Federico Rosei[‡,¶]

[‡]Institut National de la Recherche Scientifique, Énergie, Matériaux et Télécommunications, INRS, 1650, Boulevard Lionel-Boulet, Varennes, Québec J3X 1S2, Canada

[§]NAST Center & Department of Chemical Science and Technology, University of Rome, Tor Vergata Viadella Ricerca Scientifica 1, Rome 00133, Italy

[¶]Centre for Self-Assembled Chemical Structures (CSACS), McGill University, H3A Montreal, Canada

We report a power conversion efficiency of ~0.01% in multi-stacking of $BiFeO_3/BiCrO_3$ bilayer thin films used as active layers in a photovoltaic (PV) device. The films were epitaxially deposited by pulse laser deposition onto (100) oriented $CaRuO_3$-coated $LaAlO_3$ substrates and were subsequently illuminated with 1 sun (AM 1.5). The fill factor is determined to be 0.31%, a remarkable value for ferroelectric- and multiferroic-based PV devices. Our results demonstrate that photocurrent density and photovoltage can be tuned by varying the thickness and number of respective bilayers in the improvement of PV properties of multiferroic heterostructures. The maximum photocurrent is generated at an optimal multilayer thickness of 60 nm, with its origin being mainly ascribed to the contribution of ferroelectric polarization.

I. Introduction

The recent surge of interest in the optoelectronic properties in ferroelectric perovskite thin films paved the way for the exploration of new approaches for energy conversion including applications in photovoltaics (PV). Without need for n–p junction, the ferroelectric polarization of such thin films induces a strong internal electric field, which can be used to separate photo-generated carriers, thus producing a photocurrent. In addition, the total photovoltage (V_{oc}) in these materials is a series sum across areas, such as domains, yielding V_{oc} values that may exceed the band gap. Intrinsic PV properties have been discovered in numerous ferroelectric materials including $LiNbO_3$,[1,2] $BaTiO_3$,[3] and $Pb(Zr_x,Ti_{1-x})O_3$ (PZT).[4] To date, La-doped epitaxial PZT thin films have demonstrated a power conversion efficiency of up to ~0.005% under sun light.[5] However, the observed photocurrents are insignificant, of the order of nA/cm^2, mainly due to the wide band gap of ferroelectrics (typically 3–4 eV) and their high electrical resistivity. As a result, devices based on ferroelectric films as active layers are not considered promising for PV applications.

Due to the coexistence of ferroelectricity and magnetic order (i.e., transition-metal ions with unpaired d electrons), epitaxial multiferroic films[6,7] are a new material class for PV applications as they usually have strong unidirectional ferroelectric polarizations and considerably smaller band gaps (typically ~1.7–2.7 eV) compared with conventional ferroelectric materials (~3.5 eV). Recently, an encouraging power conversion efficiency of about 6% under red-light illumination (wavelength of 635 nm) in multiferroic epitaxial Bi_2FeCrO_6 (BFCO) thin films[8] and a 10% external quantum efficiency in multiferroic $BiFeO_3$ thin films were reported.[9] Furthermore, V_{oc} values of 15–28 V, which largely exceed the material's band gap (i.e., 2.75 eV), can be produced in $BiFeO_3$ thin films[10], due to a bulk PV effect.[11] A high short-circuit current density (J_{sc}) of 0.99 mA/cm^2 has so far only been reported in Bi_2FeCrO_6 thin films, where its magnitude is related to the Fe–Cr cationic ordering. Recently, a combination of $BiFeO_3$ and $BiCrO_3$ films demonstrated interesting properties: heteroepitaxial $BiFeO_3/BiCrO_3$ bilayers exhibit good ferroelectric properties and enhanced magnetism due to the interfacial magnetic coupling between Fe and Cr ions.[12] In addition, room-temperature multiferroic behavior was observed in artificial $BiFeO_3/BiCrO_3$ superlattices by Ichikawa *et al.*[13] It would thus be interesting to investigate the effect of such interface and PV conversion performance of $BiFeO_3/BiCrO_3$ heterostructures. Varying the key parameters such as thickness (x) and number (y) of $BiFeO_3$ and $BiCrO_3$ bilayers should lead toward an understanding of the mechanism underlying the PV effect observed in multiferroic thin films.

Here, we report on the PV properties of periodic multi-stacking of $BiFeO_3/BiCrO_3$ bilayers epitaxially deposited on $CaRuO_3$ (CRO)-coated $LaAlO_3$ (LAO) substrates by pulsed laser deposition (PLD). The as-prepared heterostructure exhibits remarkable light to electrical power conversion efficiencies compared with the efficiencies of the contributing single layers $BiFeO_3$ so far reported. A large photovoltage (V_{oc}) is observed when the number of vertically stacked $BiFeO_3/BiCrO_3$ bilayers is increased in the structure. We prepared and studied four samples to observe the effect of thickness and number of bilayer on PV properties [Fig. 1(a)]. Among them, 120-nm-thick $BiFeO_3$–$BiCrO_3$ multilayer-based device exhibits highest photovoltage, whereas 60-nm-thick $BiFeO_3$–$BiCrO_3$ multilayer-based device exhibits highest photocurrent.

II. Experimental Results and Discussions

Heteroepitaxial $BiFeO_3/BiCrO_3$ structures were grown on $CaRuO_3$-coated (100)-oriented $LaAlO_3$ substrate by PLD using the deposition conditions reported in Nechache *et al.*[12] The significant lattice mismatch between $BiFeO_3$ and $BiCrO_3$ with respect to $LaAlO_3$ (3.792 Å) induces a considerable compressive strain in the epitaxial growth of $BiFeO_3$ and $BiCrO_3$ films. This strain promotes the single phase of each material in a tetragonal structure.[14] The single-phase structure of the $BiFeO_3/BiCrO_3$ multilayers is evidenced by X-ray diffraction (XRD).

As displayed in Fig. 1(a), the θ–2θ scan shows no indication of the presence of additional phases other than

D. D. Viehland—contributing editor

Manuscript No. 33841. Received September 23, 2013; approved December 30, 2013.
†Author to whom correspondence should be addressed. e-mail: rosei@emt.inrs.ca; nechache@emt.inrs.ca; ruediger@emt.inrs.ca

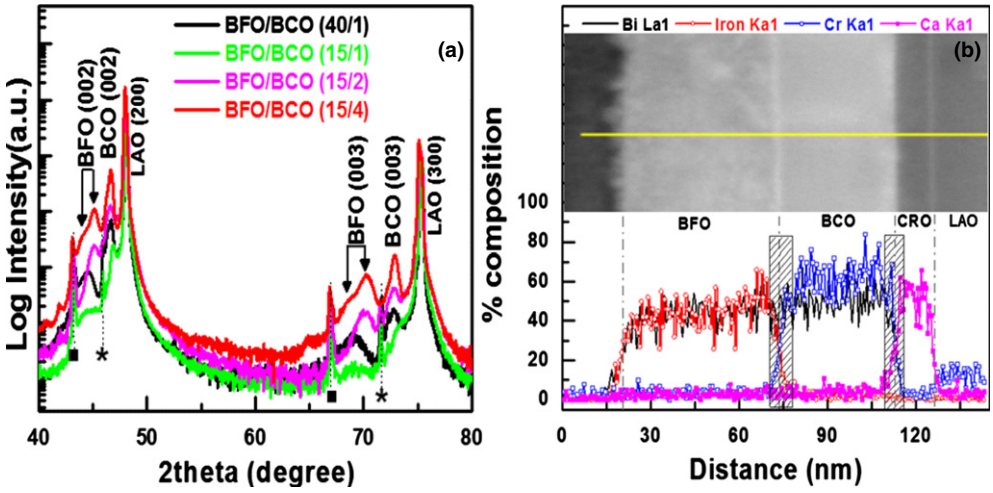

Fig. 1. (a) XRD θ–2θ scans of $BiFeO_3/BiCrO_3/CaRuO_3$ heteroepitaxial thin films grown on (100)-oriented $LaAlO_3$ substrate. x and y in $BiFeO_3$–$BiCrO_3$ (x/y) formula represent the thickness (nm) and number of layer, respectively. Squares and stars correspond to Kβ and tungsten parasitic contributions, respectively. (b) EDX Spectra of as-deposited $BiFeO_3/BiCrO_3/CaRuO_3$ bilayer film. The inset displays the corresponding low magnification cross-sectional TEM image of the heterostructure.

(001)-oriented layers. In all the grown heterostructures, the reflections from $BiFeO_3$ and $BiCrO_3$ phases can be clearly distinguished in the XRD spectra even for the structure with the highest number of bilayers. However, the XRD patterns exhibit split $BiFeO_3$ (001) reflections, suggesting the appearance of strain inhomogeneity in the heterostructure with increasing thickness.

Cross-sectional high-resolution transmission electron microscopy (HRTEM) images of the bilayer confirm that there is no deviation in the crystal orientation and the high crystal quality of each layer. Figs. 2(a) and (b) shows a typical cross-sectional HRTEM image of as-grown heterostructure deposited on (100)-oriented CRO-coated LAO substrate. It indicates the epitaxial growth of each layer on to substrate. In addition, Figs. 2(c)–(f) show diffraction pattern of corresponding fast Fourier transform of each layer. The sharp diffraction spots of each layer prove their well-developed single-crystalline structure which is in good agreement with studied XRD spectrum in the text. Figure 1(b) illustrates a typical electron-dispersive X-ray (EDX) acquired in the TEM of $BiFeO_3/BiCrO_3$ (15/1) heterostructure, where we notice the simultaneous observation of Fe and Cr at the $BiFeO_3/BiCrO_3$ interfaces.

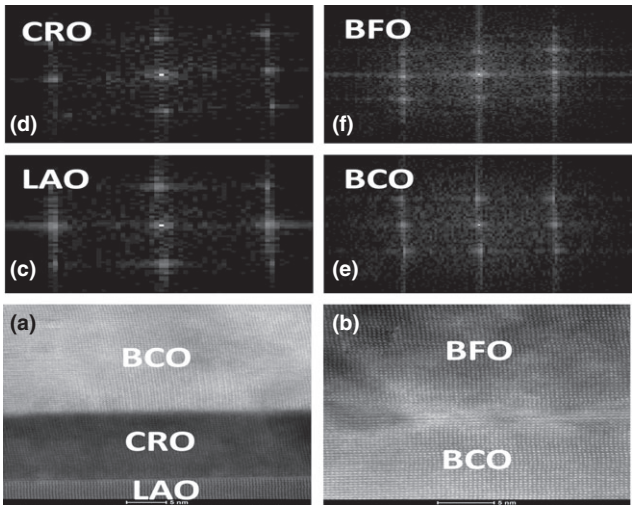

Fig. 2. High-resolution TEM image of heterostructure (a) and (b), with corresponding fast Fourier transform (c), (d), (e), and (f) of each layer individually. Scale bar is 5 nm.

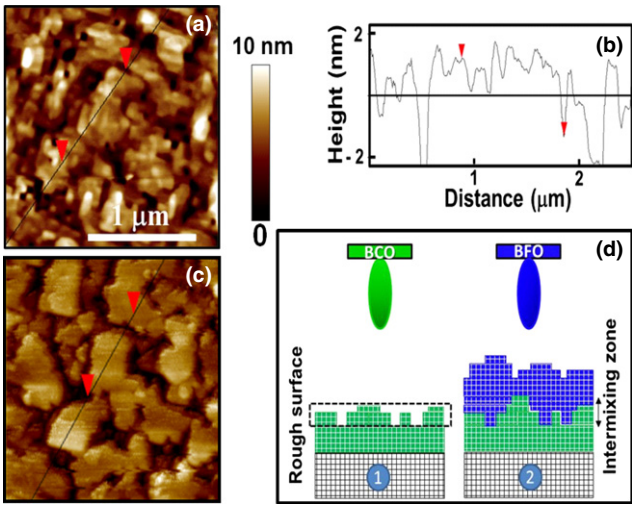

Fig. 3. (a) A 2 μm × 2 μm AFM image of the $BiCrO_3/CaRuO_3/LaAlO_3$ surface and (b) corresponding surface profile analysis. (c) AFM image of same sample after the deposition of $BiFeO_3$ layer. (d) Schematic representation illustrating the intermixing phenomenon observed during $BiFeO_3$ (BFO)/$BiCrO_3$ (BCO) bilayer deposition. The part of the scheme labeled (1) refers to the growth of the $BiCrO_3$ film characterized by a rough surface, and those labeled (2) show the sequential deposition of $BiFeO_3$ layers with the formation of an intermixing zone.

The estimated interlayer thicknesses are 7.1 nm, 6.5 nm, and 5.3 nm at $BiFeO_3/BiCrO_3$, $BiCrO_3/CaRuO_3$, and $CaRuO_3/LaAlO_3$ interfaces, respectively (with an experimental error of 5%). This apparent intermixing process is promoted by surface roughness and growth conditions, such as deposition time and substrate temperature. A typical Atomic force microscopy (AFM) topographic image of the first $BiCrO_3$ layer is illustrated in Fig. 3(a). AFM imaging shows that this film is characterized by a rough surface with rms and peak to valley values of 1.5 and 4.5 nm, respectively. The heterostructure surface remains rough even after depositing the $BiFeO_3$ layer, as illustrated in Fig. 3(c). Such surfaces mainly contribute to interface mixing, in particular when 2D film growth conditions are not reached as schematically represented in Fig. 3(d). This intermixing phenomenon is observed in numerous complex metastable alloys or solid solutions obtained by sequential PLD[15,16] and in semiconductors such as Germanium/Silicon systems.[17–21] This inter-

mixing phenomena (between iron and chromium at the interface) might lead to the formation of Bi_2FeCrO_6 active layer, but there is no conclusive experimental evidence of this new phase formation that can be shown here.

The PV properties of the $BiFeO_3/BiCrO_3$ heterostructures were investigated by performing current (I)–voltage (V) measurements both in dark and under sun simulator with maximum power density of 100 mW/cm^2 (AM 1.5 filter). The measurements were performed in both unpoled and poled conditions by applying an appropriate potential between top and bottom electrodes. Two-dimensional arrays of indium tin oxide (ITO) films deposited by PLD through a shadow mask were used as top electrodes, shown in Fig. 4(a).

The geometry of the tested structures and current density (J)–voltage (V) curves of all unpoled samples are shown in Fig. 4. Among them, the sample with four alternating, each layer of 15 nm, of $BiFeO_3/BiCrO_3$ bilayers [i.e., $BiFeO_3/BiCrO_3$ (15/4)] exhibits the highest V_{oc} (~1.2 V) which decreases linearly in magnitude as the number of incorporation of bilayers is reduced in the structure [cf. Fig. 5(a)]. Most importantly, the small J_{sc} value observed for the single bilayer [$BiFeO_3/BiCrO_3$ (40/1)] becomes more significant when the layer thickness is reduced [$BiFeO_3/BiCrO_3$ (15/1)]. The highest J_{sc} value of ~0.013 mA/cm^2 is recorded in $BiFeO_3/BiCrO_3$ (15/2).

There are two likely scenarios that can describe the origin of the experimentally observed PV effect. The first one is the effect of Schottky barrier at electrode–film interface that would depend on the alignment of Fermi levels and the second one is the bulk PV effect. The formation of a Schottky barrier at the ITO–$BiFeO_3$ interface can separate the photo-induced charge carriers effectively.[9] The second one involves the role of the ferroelectric polarization as a driving force for charge separation within the device. The overall PV effect originates from the combined superposition of both.

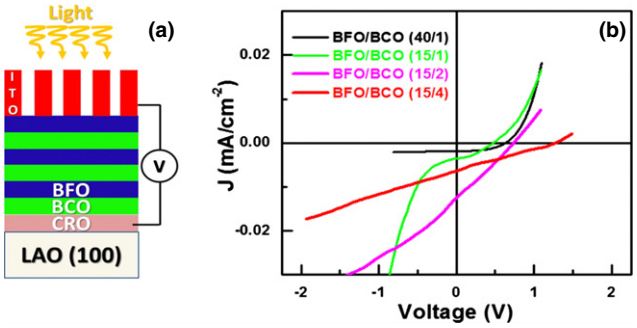

Fig. 4. (a) Geometry of tested structure involving $BiFeO_3/BiCrO_3$ bilayers. (b) J–V measurement curves revealing PV effect in $BiFeO_3/BiCrO_3$ heteroepitaxial films.

To estimate the contribution of ferroelectric polarization to the PV effect in our J–V measurement curve conducted on $BiFeO_3/BiCrO_3$ (15/4), we used a microsecond pulse of ±15 V to achieve positive and negative poling of the film, respectively. After each poling, J–V measurement was performed, shown in Fig. 5(b). The red curve in Fig. 5(b) shows that the value of the short-circuit photocurrent and photovoltage increases compared with the observed photocurrent and photovoltage in Fig. 4(b). This improvement of the photocurrent and photovoltage taken after polarization switching is attributed to a higher degree of domain alignment.[22] The as-grown heterostructures exhibit no preferential ferroelectric domain orientations [cf. right inset of Fig. 5(b)] as revealed by piezoresponse force microscopy (z-PFM). At local scale, the ferroelectric domains can be individually or partially switched by ±5 V voltage pulses. However, in a macroscopic measurement, the film became down poled after applying a −15 V pulse. Under such conditions, the polarization is oriented toward the bottom electrode (connected with substrate), and the depolarized field (E_{dp}) is oriented toward the top electrode.[23] As a result, a negative J_{sc} (~0.013 mA/cm^2) was recorded. The reverse phenomenon was observed after +15 V pulses and measuring a positive J_{sc} around ~0.008 mA/cm^2.

The J–V curve taken at the state of negative and positive poling reveals that the two J_{sc} values (differences between zero crossing of x–y-axis and the crossing of J–V curve and y-axis in poled and unpoled state) are not of identical absolute value. This relates to the fact that the total PV effect also contains the electrode–film interface contribution. Similar to Zheng *et al.*[23], we found that the ferroelectric polarization-induced internal electric field represents a major contribution (~70%) to the observed PV effect. A maximum power conversion efficiency is obtained from $BiFeO_3/BiCrO_3$ (15/4) films, of the order of 0.01% with a fill factor (FF) of about 0.31 [FF = $P_{out}^{max}/(V_{oc}*J_{sc})$].

The observed PV phenomena, i.e., variation in current density and open circuit voltage in all devices, can be described by absorption of solar spectrum as a function of penetration depth. According to Lambert–Beer's law, the intensity of light decreases exponentially with the depth inside the material. The absorption depth is given by the inverse of the absorption coefficient or α^{-1}. The absorption depth gives the distance into the material at which the light drops to about 36% of its original intensity. In particular, the penetration depth is wavelength dependent. As the optical direct band gaps of $BiFeO_3$ (~2.77 eV)[24] and $BiCrO_3$ (~2.95 eV)[25] are similar, we assume a homogeneous band gap for the whole volume of the structure. However, the thickness of the samples depends on number of bilayer. $BiFeO_3/BiCrO_3$ (15/2) exhibits a higher photocurrent mainly due to the higher absorption spectrum, suggesting that the device with a multilayer thickness of 60 nm is optimal among other

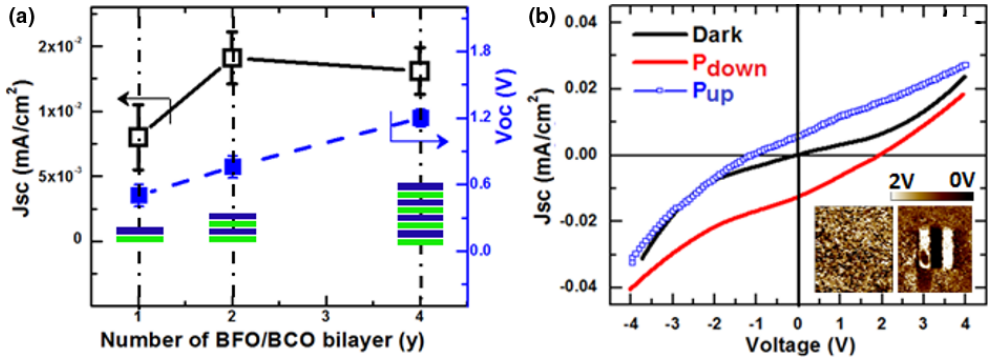

Fig. 5. (a) Evolution of main PV parameters with number of $BiFeO_3/BiCrO_3$ bilayers. (b) PV properties of the $BiFeO_3/BiCrO_3$ (15/4) heterostructures after applying pulse bias of ±15 V. The inset shows z-PFM image (5 μm × 5 μm) with constant applied voltage and variable (±5 V) applied voltage, respectively, confirming the switching of ferroelectric polarization.

devices. In the case of $BiFeO_3/BiCrO_3$ (15/4), first two bilayers contribute toward maximum photocharge carrier generation, whereas the photocarrier generation in bottom bilayers decreases.

Future studies will investigate the role of the $BiFeO_3$–$BiCrO_3$ interface in the formation of Bi_2FeCrO_6 with an even smaller band gap and enhanced bulk PV properties. Additional experiments on kinetics versus thermodynamics during film growth are required to better describe the formation of the interface. Raman scattering and optical absorption measurement are expected to establish the nature and type of interface forms and to address its effect on PV characteristics.

III. Conclusion

In summary, we demonstrated the tunability of photocurrent density and photovoltage by tailoring the thickness and number of $BiFeO_3/BiCrO_3$ bilayers in the overall heterostructure. A maximum PV power conversion efficiency (~0.01%) is observed in samples with the highest number of bilayers. This is mainly due to the linear increase in photovoltage with the stacking number of $BiFeO_3/BiCrO_3$ bilayers. A progressive absorption with increasing penetration depth is invoked to explain the behavior of observed photocurrent density and photovoltage in the films. Future work will involve Raman scattering[26,27] and absorption measurements, to investigate in depth the nature and properties of the interlayer formed at the $BiFeO_3/BiCrO_3$ interface.

Acknowledgments

We acknowledge infrastructure support from the Canada Foundation for Innovation. F. R. is grateful to the Canada Research Chairs Program for partial salary support. A. R. and F. R. are supported by FQRNT Team Project (Quebec) and by individual Discovery Grants (NSERC). F. R. thank MDEIE (Quebec) for an international collaboration grant. S. L. is supported by CSC and FQRNT graduate fellowships. We are grateful to L. Gunawan and G. A. Botton from McMaster University for the EDX analysis. R. N. acknowledges NSERC for a personal postdoctoral fellowship for partial salary support.

References

[1]A. M. Glass, D. von der Linde, and T. J. Negran, "High-Voltage Bulk Photovoltaic Effect and the Photorefractive Process in $LiNbO_3$," *Appl. Phys. Lett*., **25** [4] 233–5 (1974).

[2]A. M. Glass, D. Von der Linde, D. H. Auston, and T. J. Negran, "Excited State Polarization, Bulk Photovoltaic Effect and the Photorefractive Effect in Electrically Polarized Media," *J. Electron. Matter*, **4** [5] 915–43 (1975).

[3]V. M. Fridkin and B. N. Popov, "Anomalous Photovoltaic Effect in Ferroelectrics," *Sov. Phys. Usp*., **21**, 981–94 (1978).

[4]P. S. Brody and F. Crowne, "Mechanism for the High Voltage Photovoltaic Effect in Ceramic Ferroelectrics," *J. Electron. Matter*, **4** [5] 955–71 (1975).

[5]M. Qin, K. Yao, and Y. C. Liang, "High Efficient Photovoltaics in Nanoscaled Ferroelectric Thin Films," *Appl. Phys. Lett*., **93** [12] 122904, 3pp (2008).

[6]J. Wang, J. B. Neaton, H. Zheng, V. Nagarajan, S. B. Ogale, B. Liu, D. Viehland, V. Vaithyanathan, D. G. Schlom, U. V. Waghmare, N. A. Spaldin, K. M. Rabe, M. Wuttig, and R. Ramesh, "Epitaxial $BiFeO_3$ Multiferroic Thin Film Heterostructures," *Science*, **299**, 1719–22 (2003).

[7]R. Nechache, C. Harnagea, A. Pignolet, F. Normandin, T. Veres, L.-P. Carignan, and D. Ménard, "Growth, Structure, and Properties of Epitaxial Thin Films of First-Principles Predicted Multiferroic Bi_2FeCrO_6," *Appl. Phys. Lett*., **89** [10] 102902, 3pp (2006).

[8]R. Nechache, C. Harnagea, S. Licoccia, E. Traversa, A. Ruediger, A. Pignolet, and F. Rosei, "Photovoltaic Properties of Bi_2FeCrO_6 Epitaxial Thin Films," *Appl. Phys. Lett*., **98** [20] 202902, 3pp (2011).

[9]S. Y. Yang, L. W. Martin, S. J. Byrnes, T. E. Conry, S. R. Basu, D. Paran, L. Reichertz, J. Ihlefeld, *et al*., "Photovoltaic Effects in $BiFeO_3$," *Appl. Phys. Lett*., **95** [6] 062909, 3pp (2009).

[10]S. Y. Yang, J. Seidel, S. J. Byrnes, P. Shafer, C. -H. Yang, M. D. Rossell, J. F. Scott, J. W. Ager, *et al*., "Above-Bandgap Voltages from Ferroelectric Photovoltaic Devices," *Nat. Nanotechnol*., **5**, 143–7 (2010).

[11]M. Alexe and D. Hesse, "Tip-Enhanced Photovoltaic Effects in Bismuth Ferrite," *Nat. Commun*., **2**, 256, 5pp (2011).

[12]R. Nechache, P. Gupta, C. Harnagea, and A. Pignolet, "Enhanced Magnetism in Epitaxial $BiFeo_3/BiCro_3$ Multiferroic Heterostructures," *Appl. Phys. Lett*., **91** [22] 222908, 3pp (2007).

[13]N. Ichikawa, M. Arai, Y. Imai, K. Hagiwara1, H. Sakama, M. Azuma, Y. Shimakawa, M. Takano, Y. Kotaka, M. Yonetani, H. Fujisawa, M. Shimizu, K. Ishikawa, and Y. Chao, "Multiferroism at Room Temperature in $BiFeO_3$/$BiCrO_3$(111) Artificial Superlattices," *Appl. Phys. Exp*., **1**, 101302, 3pp (2008).

[14]H. Béa, M. Bibes, S. Fusil, K. Bouzehouane, E. Jacquet, K. Rode, P. Bencok, and A. Barthélémy, "Investigation on the Origin of the Magnetic Moment of $BiFeO_3$ Thin Films by Advanced X-Ray Characterizations," *Phys. Rev. B*, **74** [2] 020101, 4pp (2006).

[15]D. H. Kim, H. N. Lee, M. D. Biegalski, and H. M. Christen, "Large Ferroelectric Polarization in Antiferromagnetic $BiFe_{0.5}Cr_{0.5}O_3$ Epitaxial Films," *Appl. Phys. Lett*., **91** [4] 042906, 3pp (2007).

[16]H. M. Christen, D. P. Norton, L. A. Géa, and L. A. Boatner, "Pulsed Laser Deposition of Solid-Solution Films Using Segmented Targets," *Thin Solid Films*, **312** [1-2] 156–9 (1998).

[17]F. Ratto and F. Rosei, "Order and Disorder in the Heteroepitaxy of Semiconductor Nanostructures," *Mater. Sci. Eng., R*, **70** [1-3] 243–64 (2010).

[18]F. Ratto, S. Heun, O. Moutanabbir, and F. Rosei, "*In Situ* Nanoscale Mapping of the Chemical Composition of Surfaces and 3D Nanostructures by Photoelectron Spectromicroscopy," *Nanotechnology*, **19**, 265703, 7pp (2008).

[19]F. Ratto, G. Costantini, A. Rastelli, O. G. Schmidt, K. Kern, and F. Rosei, "Alloying of Self-Organized Semiconductor 3D Islands," *J. Exp. Nanosci*., **1** [3] 279–305 (2006).

[20]F. Ratto, A. Locatelli, S. Fontana, S. Kharrazi, S. Ashtaputre, S. K. Kulkarni, S. Heun, and F. Rosei, "Chemical Mapping of Individual Semiconductor Nanostructures," *Small*, **2** [3] 401–5 (2006).

[21]N. Motta, F. Rosei, A. Sgarlata, G. Capellini, S. Mobilio, and F. Boscherini, "Evolution of the Intermixing Process in Ge/Si(111) Self-Assembled Islands," *Mat. Sci. Eng. B*, **88**, 264–8 (2002).

[22]M. Qui, K. Yao, and Y. C. Liang, "Photovoltaic Characteristics in Polycrystalline and Epitaxial $(Pb_{0.97}La_{0.03})(Zr_{0.52}Ti_{0.48})O_3$ Ferroelectric Thin Films Sandwiched between Different Top and Bottom Electrodes," *J. Appl. Phys*., **105** [6] 061624, 7pp (2009).

[23]F. Zheng, J. Xu, L. Fang, M. Shen, and X. Wu, "Separation of the Schottky Barrier and Polarization Effects on the Photocurrent of Pt Sandwiched $Pb(Zr_{0.20}Ti_{0.80})O_3$ Films," *Appl. Phys. Lett*., **93** [17] 172101, 3pp (2008).

[24]A. Kumar, R. C. Rai, N. J. Podraza, S. Denev, M. Ramirez, Y. Chu, L. W. Martin, J. Ihlefeld, *et al*., "Linear and Nonlinear Optical Properties of $BiFeO_3$," *Appl. Phys. Lett*., **92** [12] 121915, 3pp (2008).

[25]C. Himcinschi, L. Vrejoiu, T. Weißbach, K. Vijayanandhini, A. Talkenberger, C. Roder, S. Bahmann, D. R. T. Zahn, *et al*., "Raman Spectra and Dielectric Function of $BiCrO_3$: Experimental and First-Principles Studies," *J. Appl. Phys*., **110** [7] 073501, 8pp (2011).

[26]J. Andreasson, J. Holmlund, S. G. Singer, C. S. Knee, R. Rauer, B. Schulz, M. Käll, M. Rübhausen et al, "Electron-Lattice Interactions in the Perovskite $LaFe_{0.5}Cr_{0.5}O_3$ Characterized by Optical Spectroscopy and LDA+U Calculations," *Phys. Rev. B*, **80** [7] 075103, 5pp (2009).

[27]J. Andreasson, J. Holmlund, R. Rauer, M. Käll, L. Börjesson, C. S. Knee, A. K. Eriksson, S.-G. Eriksson, *et al*., "Electron-Phonon Interactions in Perovskites Containing Fe and Cr Studied by Raman Scattering using Oxygen-Isotope and Cation Substitution", *Phys. Rev. B*, **78** [23] 235103, 13pp (2008). □